Received: 9 May 2023 | Revised: 4 September 2023 | Accepted: 21 September 2023

DOI: 10.1002/cac2.12490

CANCER COMMUNICATIONS Open Access

LETTER TO THE EDITOR

Targeted STAT1 therapy for LZTR1-driven peripheral nerve sheath tumor

Dear Editor,

Schwannomas are peripheral nervous system tumors that cause chronic pain, numbness, and potentially life-threatening organ dysfunction. Surgery is a conventional treatment for schwannoma patients. However, those who undergo surgery may experience neurological deficits. Moreover, the management of schwannomas can be problematic due to their unpredictable growth. Thus, there is a pressing need for nonsurgical treatments to manage both tumor growth and pain control.

Germline mutations of leucine zipper like post-translational regulator 1 (*LZTR1*), a 22q tumor suppressor gene, account for approximately 30% of all non-NF2-related schwannomatosis cases [1]. *LZTR1* loss is associated with mitogen-activated protein kinases (MAPK)1 activation [2]. Given that standard clinical trials are exceedingly difficult for schwannoma patients, mouse models offer the possibility of bespoke therapeutic regimens. Only a few animal models of schwannomatosis exist in mice, as only a model combining *Lztr1* and cyclin-dependent kinase inhibitor 2A (*Cdkn2A*) mutations in the nervous system using a Glial fibrillary acidic protein-driven Cre recombinase was reported [3], highlighting a need for models that faithfully recapitulate *LZTR1*-mutated schwannoma, using proper Schwann cell-specific promoters.

Abbreviations: [^{18}F]-FDG, ^{18}F-fluorodeoxyglucose; +, wild type; Bcl-xL, B-cell lymphoma-extra-large; CCL2, C-C Motif Chemokine Ligand 2; CCL2, C-C motif chemokine ligand; Ccnd1, cyclin D1; Cdk2A, cyclin-dependent kinase inhibitor 2A; F4/80 (EMR1), EGF-like module-containing mucin-like hormone receptor-like 1; Fl, flox allele; GFP, Green Fluorescent protein; HEI-193, House Ear Institute 193; IL6, Interleukin 6; IL8, Interleukin 8; Ki67, marker of proliferation Ki67; LATS1, large tumor suppressor kinase 1; LATS2, large tumor suppressor kinase 2; LZTR1, leucine zipper like post-translational regulator 1; MERLIN, moesin-ezrin-radixin-like tumor suppressor; MAPK, Mitogen-activated protein kinases; Mpz, myelin protein zero; NF2, neurofibromatosis type 2; OLIG4, oligodendrocyte marker O4; PET-CT, Positron Emission Tomography and Computed Tomography; sh, short hairpin; SOX2, SRY-box transcription factor 2; STAT1, signal transducer and activator of transcription 1.

To model germline *Lztr1* loss of function, we induced *Lztr1* knockout in Schwann cell precursors using a Cre recombinase (cre) driven by the myelin protein zero (P0) (*Mpz*) promoter. We observed a decrease in *Lztr1* expression in oligodendrocyte marker O4 (OLIG4)-positive Schwann cells from *P0 cre Lztr1*$^{flox\ allele\ (fl);fl}$ mice, confirming the specific deletion of *Lztr1* in Schwann cells (Supplementary Figure S1A-B). However, we did not detect any phenotypic changes in the *Mpz*-specific *Lztr1* knockout mice (Figure 1A), which could be explained by the fact that germline *LZTR1* mutations in patients are frequently accompanied by a somatic 22q chromosomal region loss, containing *LZTR1* and the other 22q tumor suppressors, such as Neurofibromatosis type 2 (*NF2*) and SWI/SNF related, matrix associated, actin dependent regulator of chromatin subfamily B member 1 (*SMARCB1*) [4]. *NF2* encodes a moesin-ezrin-radixin-like tumor suppressor (MERLIN), which negatively regulates the Hippo pathway through large tumor suppressor kinases, LATS1 and LATS2. Either Schwann-cell specific *Nf2* or a double *Lats1/2* knockout leads to schwannomatogenesis in mice [5, 6], whereas MAPK signaling has been proposed as a modifier of schwannoma formation [5].

To model *LZTR1*-mutant schwannoma development in humans, we generated a Schwann cell-specific triple *Lztr1, Lats1, and Lats2* knockout mice. Although in the *P0 cre Lztr1*$^{fl;fl}$*; Lats1/2*$^{fl;+}$ mice, the loss of *Lztr1* and *Lats1/2* is not sequential, our model partially recapitulates the *LZTR1*-mutant schwannoma occurring in patients. We observed sporadic unilateral sciatic, nasofacial, and peripheral nerve schwannomas in *P0 cre Lztr1*$^{+;+}$ *Lats1/2*$^{fl;+}$ and *P0 cre Lztr1*$^{fl;fl}$ *Lats1/2*$^{fl;+}$ mice (Supplementary Figure S1C-E). Hence, our model partially recapitulates schwannoma development, which also appears sporadically and displays unpredictable clinical behavior in patients.

To unbiasedly detect Schwann cell-derived tumors, we performed magnetic resonance imaging on 30-week-old mice. Vestibulocochlear nerve enlargement was detected in the *P0 cre Lztr1*$^{fl;fl}$ *Lats1/2*$^{fl;+}$ when compared to the *P0 cre Lztr1*$^{fl;fl}$ *Lats1/2*$^{+;+}$ and *P0 cre Lztr1*$^{+;+}$ *Lats1/2*$^{fl;+}$

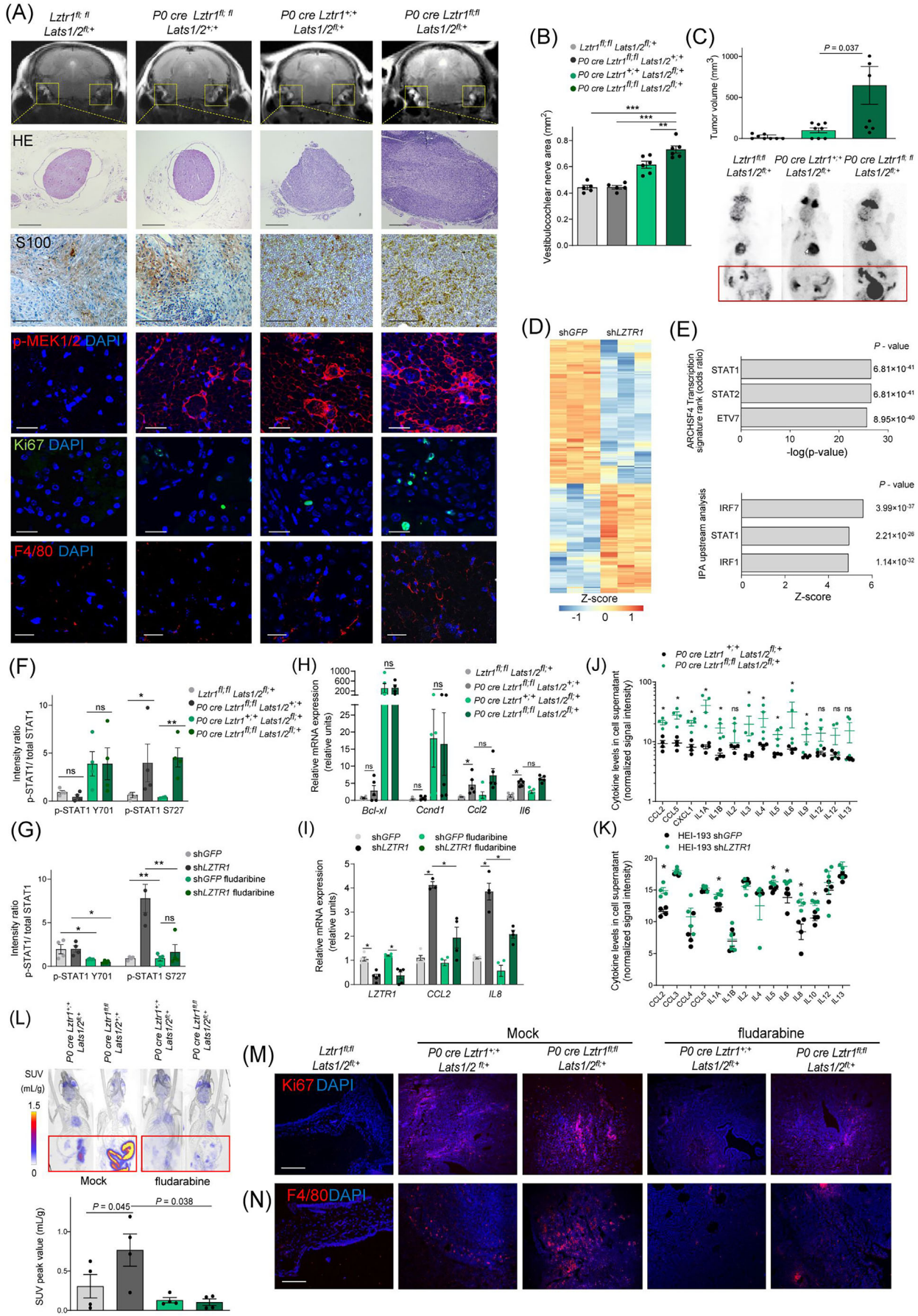

mice (Figure 1A-B). We also detected tumor masses in the abdomen of 100-week-old mice using a positron emission tomography-computed tomography (PET-CT) scan with ^{18}F-fluorodeoxyglucose ([^{18}F]-FDG) (Figure 1C). Male *P0 cre Lztr1*$^{fl;fl}$ *Lats1/2*$^{fl;+}$ mice developed seminal vesicle Schwann-cell-derived tumors (Supplementary Figure S1F) that mimic rare prostate-type schwannomas [7]. Female *P0 cre Lztr1*$^{fl;fl}$ *Lats1/2*$^{fl;+}$ mice presented cervical Schwann-cell-derived tumors (Supplementary Figure S1G) that approximate rare uterus-derived schwannomas [8]. Volumetric analysis of PET-CT scans with [^{18}F]-FDG revealed that loss of *Lztr1* was associated with higher metabolic activity and increased tumor burden (Figure 1C). Tumor origin was confirmed by S100 and SRY-box transcription factor 2 (SOX2) immunostainings (Figure 1A, Supplemental Figures S1H-I).

Concordant to previous reports [2], immunohistochemical analysis of isolated vestibulocochlear nerves revealed that *Lztr1* loss led to increased phosphorylation of mitogen-activated protein kinase MEK1/2 in both wild-type and *Lats1/2*-knockout mice (Figure 1A). Similarly, we observed an activation of extracellular signal-regulated kinases 1/2 (ERK1/2) upon *LZTR1* depletion in *NF2*-mutated schwannoma cell line HEI-193 (Supplementary Figure S2A). Moreover, immunohistochemical analysis of vestibulocochlear nerves isolated from the triple knockout mice also revealed increased cell proliferation and higher levels of macrophage infiltration as detected by Ki67 and F4/80 immunostainings, respectively (Figure 1A, Supplementary Figure S2B). This indicates that concurrent loss of *Lztr1* and *Lats1/2* could promote schwannoma development intrinsically as well as by altering the tumor microenvironment, which is commonly observed during schwannoma progression in patients [9].

To investigate *LZTR1*-mediated molecular alterations promoting schwannomatosis, we performed proteomics analysis of human Schwann cells expressing either sh*GFP* or sh*LZTR1* (Figure 1D). The upstream regulator analyses of the differentially expressed proteins (Supplementary Table S1) showed the activation of the signal transducer and activator of the transcription 1 (STAT1) pathway triggered by *LZTR1* depletion (Figure 1E), suggesting the contribution of the STAT1 pathway to LZTR1-mediated disease pathogenesis. STAT1 function is regulated through phosphorylation on Y701 by Janus kinases (JAK) and S727 by MAPK kinases [10]. We found that the *Lats1/2* co-deletion induced phosphorylation of STAT1 on Y701 but not on S727 (Figure 1F, Supplementary Figure S2C). In contrast, *LZTR1* depletion in *Lats1/2* knockout mouse Schwann cells or *NF2*-mutant HEI-193 cells increased the phosphorylation of STAT1 on S727 (Figure 1F-G, Supplementary Figure S2D), suggesting that LZTR1-mediated increase in the MAPK activity modulates STAT1 function by inducing its phosphorylation on S727.

LATS1/2-regulated phosphorylation of Y701 led to increased expression of well-known STAT1 transcriptional targets B-cell lymphoma-extra-large (*Bcl-xL*) and cyclin D1 (*Ccnd1*) (Figure 1H). On the other hand, phosphorylation at both sites in the triple knockout cells induced transcription of additional STAT1 targets, such as

FIGURE 1 The role of LZTR1 in peripheral nerve tumor progression. **(A)** T2-weighted MRI imaging of 30-week-old mice. The yellow boxes indicate the vestibulocochlear nerve. H&E staining was performed on the isolated vestibulocochlear nerve of the same mice. Scale bar: 1 mm and 100 μm. Immunostaining for S100, F4/80, phosphorylated MEK1/2 (p-MEK1/2), and Ki-67 of the vestibulocochlear nerves. Scale bar: 100μm and 30 μm, respectively. **(B)** Quantification of the vestibulocochlear nerve area based on the T2-weighted MRI images. $n = 6$ per group. **(C)** Maximum intensity projection PET-CT images of 100-week-old mice after [^{18}F]-FDG injection. The tumor volume in the abdominal area was quantified using PET-CT volumes. $n = 8$ per group. **(D)** Heatmap of proteins differentially expressed in human primary Schwann cells expressing sh*GFP* or sh*LZTR1*. $n = 3$ per group. **(E)** ARCHSF4 and IPA upstream analyses of the differentially expressed proteins. **(F)** Analysis of OLIG4-positive cells isolated from the sciatic nerves by immunoblotting. Values are means of phosphorylated relative to total STAT1 levels ± SEM. $n = 4$ per group. **(G)** Analysis of HEI-193 cells expressing sh*GFP* or sh*LZTR1* treated with fludarabine (0.01 mmol/L, 48 hours) by immunoblotting. Values are means of phosphorylated (p) relative to total STAT1 levels. $n = 4$ per group. **(H)** Quantification of mRNA expression in OLIG4-positive cells isolated from the sciatic nerve. $n = 5$ per group. **(I)** Quantification of mRNA expression in HEI-193 cells treated with fludarabine (0.01 mmol/L, 48 hours). $n = 4$ per group. **(J)** Secretome analysis of OLIG4-positive cells isolated from the sciatic nerves. $n = 5$ per group. **(K)** Secretome analysis of HEI-193 cells expressing sh*GFP* or sh*LZTR1*. $n = 5$ per group. **(L)** PET-CT images of 100-week-old mice injected with [^{18}F]-FDG after treatment with fludarabine (100 mg/kg, 14 days every 2 days). SUV-scaled tracer uptake quantification in the abdomen. $n = 4$ per group. **(M, N)** Immunohistochemical analysis for Ki67 and F4/80 expression in the uterus schwannomas after treatment with fludarabine (100 mg/kg, 14 days every 2 days). Scale bar: 100 μm. Data are shown as mean ± SEM. ***B, C, J, K*** and ***L***, *P* values: Wilcoxon Mann-Whitney test. ***F, G*** **and** ***H***, *P* values: Mann Whitney test. * $P \leq 0.05$, ** $P \leq 0.01$, and *** $P \leq 0.001$. Abbreviations: [^{18}F]-FDG, ^{18}F-fluorodeoxyglucose; +, wild type; ARCHSF4, All RNA-seq and ChIP-seq sample and signature search; F4/80 (EMR1), EGF-like module-containing mucin-like hormone receptor-like 1; Fl, flox allele; GFP, Green Fluorescent Protein; HEI-193, House Ear Institute 193; IPA, Ingenuity Pathway Analysis; Ki67, marker of proliferation Ki67; LZTR1, leucine zipper like post-translational regulator; MEK1/ 2, mitogen-activated protein kinase 1/ 2; MRI, magnetic resonance imaging; ns, not significant; PET-CT, Positron Emission Tomography and Computed Tomography; OLIG4, oligodendrocyte marker O4; SEM, standard error of the mean; sh, short hairpin; STAT1, signal transducer and activator of transcription 1; SUV, standardized uptake value.

pro-immunogenic secreted factors, C-C motif chemokine ligand (*CCL2*) and interleukin 6 (*IL6*)/ interleukin 8 (*IL8*) (Figure 1H-I). Concordantly, the cytokine array analysis revealed an increased secretion of multiple cytokines by the *P0 cre Lztr1*$^{fl;fl}$ *Lats1/2*$^{fl;+}$ mouse-isolated Schwann cells (Figure 1J). Similarly, *LZTR1* depletion in the HEI-193 cells increased secretion of IL6, IL8, and CCL2 (Figure 1K). The STAT1 inhibitor fludarabine suppressed STAT1 phosphorylation at both sites and decreased *CCL2* and *IL8* expression (Figure 1G, I). Inhibition of the STAT signaling by either fludarabine or nifuroxazide also abolished the increased secretion of IL6 and IL8 induced by *LZTR1* depletion (Supplementary Figure S2E). These results indicate that depletion of the LATS1/2 kinases triggers STAT1-induced expression of cell proliferation and survival regulators, whereas concurrent LZTR1 loss results in a STAT1-dependent increase in cytokine production.

We next assessed the therapeutic effect of STAT1 inhibition for schwannoma treatment. We found that in vivo treatment with fludarabine led to a significant decrease of [^{18}F]-FDG uptake by sexual tissue-derived nerve sheath tumors (Figure 1L). Immunohistochemistry analysis confirmed that STAT1 inhibition led to decreased tumor cell proliferation and lower macrophage infiltration within the tumor environment as detected by Ki67 and F4/80 immunostainings, respectively (Figure 1M-N, Supplementary Figure S2F). These results indicate that STAT1 activation contributes to schwannomatosis via both tumor cell-intrinsic and extrinsic mechanisms. The synergistic effect of the Hippo and MAPK pathway activities upregulates a broader range of STAT1 target genes, resulting in both pro-proliferative and pro-inflammatory phenotypes (Supplementary Figure S2G).

In summary, we demonstrated that LZTR1-mediated activation of the MAPK cascade leads to the phosphorylation of STAT1 at S727, whereas LATS1/2 loss promotes the phosphorylation of STAT1 at Y701. Anti-STAT1 therapy decreased inflammation and tumor cell proliferation in schwannomas. These results identified anti-STAT1 therapy as a potential strategy for schwannomas with the loss of *LZTR1* function.

DECLARATIONS

AUTHOR CONTRIBUTIONS

Tonci Ivanisevic and Raj N Sewduth performed the in vivo and in vitro experiments; Mikhail Steklov performed the sample preparation for Mass Spectrometry; Benoit Lechat performed the genotyping and cloning; Christopher Cawthorne performed the PET-CT under the supervision of Christophe Deroose and Koen Van Laere; Christophe Deroose and Koen Van Laere provided the tracer for PET-CT; Tonci Ivanisevic performed the CT-scan under the supervision of Greetje Vande Velde; Willy Gsell performed the MRI under the supervision Uwe Himmelreich; the data analysis was performed by Tonci Ivanisevic, Raj N Sewduth under the supervision of Anna A Sablina, Christopher Cawthorne, Greetje Vande Velde and Uwe Himmelreich; Raj N Sewduth, Anna A Sablina wrote the paper and designed the figures.

ACKNOWLEDGMENTS

We thank Dr. Jeremie Vitte and Prof. Marco Giovannini (University of California, Los Angeles) for providing comprehensive training for Tonci Ivanisevic and gifting the HEI-193 cells. We thank Prof. Georg Halder (VIB-KU Leuven Center for Cancer Biology) for gifting transgenic *Lats1*$^{fl/+}$; *Lats2*$^{fl/+}$ mice. We also thank Jens Wouters (Nuclear Medicine and Molecular Imaging, Department of Imaging and Pathology, KU Leuven) for the help with the MRI acquisition.

CONFLICT OF INTEREST STATEMENT

All authors declare no conflicts of interest.

FUNDING INFORMATION

This research was supported by Ub-RASdisease (AS, H2020 ERC, Grant agreement ID: 772649) and the Young Investigator Award (TI, CTF, award ID: 2022-01-004).

ETHICS APPROVAL AND CONSENT TO PARTICIPATE

All procedures involving animals were performed following the guidelines of the KU Leuven institutional animal care and use committee and approved in the project application 179/2020, titled 'Role of the ubiquitin system in nerve sheath cancer'.

CONSENT FOR PUBLICATION

Not applicable.

DATA AVAILABILITY STATEMENT

All the data are available upon request from the corresponding author.

Tonci Ivanisevic[1]
Mikhail Steklov[1]
Benoit Lechat[1]
Christopher Cawthorne[2]
Willy Gsell[3]
Greetje Vande Velde[3]
Christophe Deroose[2]
Koen Van Laere[2]
Uwe Himmelreich[3]
Raj N Sewduth[1]
Anna A Sablina[1]

[1]*VIB-KU Leuven Center for Cancer Biology, VIB, Leuven, Belgium*
[2]*Nuclear Medicine and Molecular Imaging, Department of Imaging and Pathology, KU Leuven, Leuven, Belgium*
[3]*Biomedical MRI, Department of Imaging and Pathology, KU Leuven, Leuven, Belgium*

Correspondence
Anna A Sablina and Raj N Sewduth, VIB-KU Leuven Center for Cancer Biology, VIB, Leuven 3000, Belgium.
Email: anna.sablina@kuleuven.be and raj.sewduth@kuleuven.be

ORCID

Anna A Sablina https://orcid.org/0000-0001-9526-4014

REFERENCES

1. Dhamija R, Plotkin S, Asthagiri A, Messiaen L, Babovic-Vuksanovic D. Schwannomatosis. In: Adam MP, Mirzaa GM, Pagon RA, Wallace SE, Bean LJH, Gripp KW, et al., editors. GeneReviews((R)). Seattle (WA): 1993.
2. Steklov M, Pandolfi S, Baietti MF, Batiuk A, Carai P, Najm P, et al. Mutations in LZTR1 drive human disease by dysregulating RAS ubiquitination. Science. 2018;362(6419):1177–82.
3. Ko A, Hasanain M, Oh YT, D'Angelo F, Sommer D, Frangaj B, et al. LZTR1 Mutation Mediates Oncogenesis through Stabilization of EGFR and AXL. Cancer Discov. 2023;13(3):702–23.
4. Kehrer-Sawatzki H, Farschtschi S, Mautner VF, Cooper DN. The molecular pathogenesis of schwannomatosis, a paradigm for the co-involvement of multiple tumour suppressor genes in tumorigenesis. Hum Genet. 2017;136(2):129–48.
5. Chen Z, Li S, Mo J, Hawley E, Wang Y, He Y, et al. Schwannoma development is mediated by Hippo pathway dysregulation and modified by RAS/MAPK signaling. JCI Insight. 2020;5(20):e141514.
6. Giovannini M, Robanus-Maandag E, Niwa-Kawakita M, van der Valk M, Woodruff JM, Goutebroze L, et al. Schwann cell hyperplasia and tumors in transgenic mice expressing a naturally occurring mutant NF2 protein. Genes Dev. 1999;13(8):978–86.
7. Pereira D, Costa G, Catarino R, Correia T, Prisco R. Schwannoma of Seminal Vesicle: A Case Report. Cureus. 2022;14(12):e32986.
8. Zhang T, Wang Z, Wang R, Wu X, Zhao M, Su F. Malignant Peripheral Nerve Sheath Tumor of the Cervix. J Coll Physicians Surg Pak. 2022;32(4):S24–S27.
9. Hannan CJ, Lewis D, O'Leary C, Waqar M, Brough D, Couper KN, et al. Increased Circulating Chemokines and Macrophage Recruitment in Growing Vestibular Schwannomas. Neurosurgery. 2023;92(3):581–89.
10. Zhang Y, Cho YY, Petersen BL, Zhu F, Dong Z. Evidence of STAT1 phosphorylation modulated by MAPKs, MEK1 and MSK1. Carcinogenesis. 2004;25(7):1165–75.

SUPPORTING INFORMATION

Additional supporting information can be found online in the Supporting Information section at the end of this article.